IEEE Access
Multidisciplinary | Rapid Review | Open Access Journal

Received March 31, 2019, accepted May 27, 2019, date of publication May 30, 2019, date of current version June 17, 2019.

Digital Object Identifier 10.1109/ACCESS.2019.2919997

Color Constancy for Uniform and Non-Uniform Illuminant Using Image Texture

MD AKMOL HUSSAIN, AKBAR SHEIKH-AKBARI, AND EDWARD ABBOTT HALPIN
School of Computing, Creative Technology, and Engineering, Leeds Beckett University, Leeds LS6 3QR, U.K.
Corresponding author: Akbar Sheikh-Akbari (a.sheikh-akbari@leedsbeckett.ac.uk)

ABSTRACT Color constancy is the capability to observe the true color of a scene from its image regardless of the scene's illuminant. It is a significant part of the digital image processing pipeline and is utilized when the true color of an object is required. Most existing color constancy methods assume a uniform illuminant across the whole scene of the image, which is not always the case. Hence, their performances are influenced by the presence of multiple light sources. This paper presents a color constancy adjustment technique that uses the texture of the image pixels to select pixels with sufficient color variation to be used for image color correction. The proposed technique applies a histogram-based algorithm to determine the appropriate number of segments to efficiently split the image into its key color variation areas. The K-means^{++} algorithm is then used to divide the input image into the pre-determined number of segments. The proposed algorithm identifies pixels with sufficient color variation in each segment using the entropies of the pixels, which represent the segment's texture. Then, the algorithm calculates the initial color constancy adjustment factors for each segment by applying an existing statistics-based color constancy algorithm on the selected pixels. Finally, the proposed method computes color adjustment factors per pixel within the image by fusing the initial color adjustment factors of all segments, which are regulated by the Euclidian distances of each pixel from the centers of gravity of the segments. The experimental results on benchmark single- and multiple-illuminant image datasets show that the images that are obtained using the proposed algorithm have significantly higher subjective and very competitive objective qualities compared to those that are obtained with the state-of-the-art techniques.

INDEX TERMS Color constancy, multiple-illuminant, image segmentation, texture.

I. INTRODUCTION

The colors of objects within a digital image are determined by the intrinsic properties of the source illuminant, reflective features of the objects' surface and the sensitivity functions of the imaging device [1]. The color of the illuminant may alter the real colors of the objects within the scene. Hence, for robust color-based systems such as human-computer interaction, video analytics, object tracking, color feature extraction and digital photography, the effect of the illuminant should be removed [2], [3]. The retinex system of humans is able to observe the actual color of objects by adjusting its spectral response and distinguishing the color of the source illuminant. In contrast to human eyes, digital imaging devices are unable to efficiently filter out the effects of light sources from digital images [4], [5]. Hence, the color of the source light can significantly deteriorate the color of objects in the image. The key purpose of color constancy algorithms is to adjust the color of an image that was taken under an unknown illuminant so that the image looks as if it captured under white illuminant [6], [7].

Color constancy of a digital image can be analyzed using an image formation model. Lambertian reflectance is one the most often used models, which assumes the reflected intensity of the light is independent of the viewing angle. This model ignores the specular reflection. By assuming a Lambertian surface, the formation of an image $f = (f_R, f_G, f_B)^T$ becomes a function of three significant factors including the color of the light source $I(\lambda)$, the sensitivity function of the camera $(\rho_R(\lambda), \quad \rho_G(\lambda), \quad \rho_B(\lambda))^T$, and the reflectance property of the surface $S(\boldsymbol{x}, \lambda)$, where λ is the light wavelength and x is the spatial coordinate of the object. The formation can then be expressed as follows [8]:

$$f_c(\boldsymbol{x}) = m(x) \int_w I(\lambda)\rho_c(\lambda)S(\boldsymbol{x}, \lambda)d\lambda \tag{1}$$

where $m(x)$ refers to the Lambertian shading.

The associate editor coordinating the review of this manuscript and approving it for publication was Weiyao Lin.

This assumes that the scene is illuminated by a single light source and the perceived color of light source e depends on the $\rho(\lambda)$ and $I(\lambda)$:

$$e = \begin{pmatrix} e_R \\ e_G \\ e_B \end{pmatrix} = \int_w I(\lambda)\,\rho(\lambda)\,d\lambda \tag{2}$$

Since camera sensitivity function and the color of the light source are unknown, the color constancy becomes an under-constrained problem that requires additional assumptions to solve it.

A considerable number of color adjustment methods have been proposed over the past years, where most of them assume that the scene is lit by just one uniform light source [9]–[30]. These algorithms can be classed into four key groups: statistical-, gamut-, physics- and learning-based methods.

Statistical-based color constancy methods use the statistical color information of the image to filter out the effect of illuminant color from the image. The Gray World color constancy method [9] is an example of a statistical-based method which is based on the assumption that the average reflectance of the RGB components of a digital image are equal and representative of the gray level. The Gray World algorithm is considered one of the best-performing methods for images that have sufficient color variation [10]. However, its resulting image becomes biased toward the color of the large uniform color patch within the image [11]. Max-RGB, which is also known as the White Patch method, is another statistical-based method, which assumes maximum values of the three image color components represent perfect reflectance [12]. Lam in [13] has taken into account the fact that the human visual system is more delicate to green than red and blue colors. He proposed an algorithm that leaves the green color component of the image unchanged and adjusts the red and blue color components using the Max-RGB method. However, the data dependency of these techniques on the brightest pixels of the image often leads to erroneous results, particularly for images with lower intensity [14]. Finlayson and Trezzi [15] proposed a method, which is called Shades of Gray, that overcomes the data reliance of the above two named methods. The authors proposed a method that uses the Minkowski p-norm to perform color constancy adjustment. This method generates superior results and significantly reduces the data reliance of the technique. However, in some cases, it generates erroneous and over-saturated images. Several refinement techniques have been proposed in [16]–[18] for alleviating the uniform color areas of the image and improving the result of the aforementioned statistics-based methods. Van de Weijer *et al.* in [19] have shown that pixels within the edge areas of the image carry important color information and can be used for color constancy adjustment. They proposed a color constancy method that uses the edge pixel information and reported significant results. In [20], an extension of the Gray Edge method, which is named the Weighted Gray Edge method, was presented. This method incorporates a general weighting scheme of the Gray Edge method by utilizing various edges within the image to perform color constancy adjustment.

Gamut mapping [21] is one of the most remarkable methods. It is based on the principle that for a given light source, in a real-world scene, only a few number of its colors are observable. Various gamut mapping algorithms have been reported in [22]–[24].

Physics-based approaches are more elaborate in their operation, as the light source estimation is driven by the interaction between the source light and the objects' physical features. They assume that a plane in RGB space represents each surface's pixels. They use the interaction between these surfaces to estimate the light sources. Many physics-based color constancy methods have been reported in [25]–[28]. Most color constancy methods, including those that are reviewed above, assume that the scene is uniformly lit by only one illuminant. However, in real-life scenarios, the scene is usually lit unevenly by one or more light sources. Hence, current color constancy algorithms are incapable to fully filter out the effects of the light colors.

Researchers have proposed a range of techniques that meet the needs of color constancy adjustment methods for images that were taken from a scene that was either un-evenly lit or lit by multiple light sources [29]–[51]. These methods can be divided into groups that are based on local light estimation and fusion [29]–[34], pixel-detection-based techniques [35]–[37], Convolutional Neural Network (CNN)-based methods [42]–[47] and biologically inspired techniques [48]–[51].

A superpixel-based segmentation method was proposed in [32], which uses various sub-sampling techniques to split the image into sub-regions and determine a light-source color estimate for each resulting sub-region. Then, the algorithm combines the resulting estimates from the same category to generate a light color estimate for each pixel. Beigpour *et al.* [33] used the conditional random field algorithm, which considers both spatial distribution of local light estimates and their colors, to generate a per-pixel light source color estimate. The authors formulated a framework as an energy minimization task of the spatial distribution, which combines a few physics-based and statistics-based color constancy methods into a single color guesstimate for multiple illuminant scene. Another multiple-light-source estimation method was proposed in [34], which uses lattices of various scales of the image to calculate a per-pixel light color estimate.

Scene illuminant estimation using sets of pixels is also considered in the literature since the process of estimating local illuminants is computationally complex and may not be feasible for real-time applications [35]–[37]. Yang *et al.* [35] suggested a technique to efficiently detect gray pixels within an image using an illuminant-invariant measure in three logarithmic color channels. This method determines an estimation for the color of the light source more accurately.

In the literature, various color constancy algorithms have also been reported that attempt to perform illumination estimation without relying on the presence of particular sets of pixels [38]–[41]. A two-stage color constancy adjustment method for outdoor images was proposed by Lee *et al.*in [41]. Their algorithm casts the shadow and sunlight as two illuminants. In the first step, the algorithm determines an estimate for the sunlight and its reflectance in the whole image using an existing technique that assume the scene is lit by only one light source. In the second step, their algorithm estimates the secondary illuminant, which corresponds to shaded regions of the image, and applies a pixel-based color correction to the shaded regions of the image by calculating the RGB adjustment ratio without estimating the color of shade. Thus, the authors have proposed a way of adopting diverse color constancy approaches for primary and secondary illuminant estimation. They have demonstrated through experiment that their technique generates significantly more accurate results in terms of angular errors on outdoor images.

Several techniques use a convolutional neural network (CNN)-based color constancy approach for multiple illuminants as an alternative to the strong-assumption-based methods [42]–[47]. Bianco *et al.* [42] use a CNN that comprises of one convolutional layer, one fully connected layer, and three output nodes. This method samples the input image into non-overlapping patches and applies the histogram stretching method to neutralize the contrast of the image. The patch scores, which are attained by mining activation values of the last hidden layer, are merged to guess the color of source light. Barron [43] observed that weighting the color components of the image causes a translation in the log-chromaticity histogram of the image, which enables the use of tools such as CNN and structure prediction. Joze and Drew [44] identifies a neighboring surface from the training data by using both inadequately color-constant RGB values and texture features. The authors then integrate them as an illuminant estimation for the whole image. Aytekin *et al.* [47] proposed another CNN-based color constancy technique that estimates the chromaticity of the light by pooling local patches from an image pyramid. Their algorithm creates the image pyramid, which consists of a few scales of the input image, and extracts local patches from all resolutions. Then, algorithm trains a CNN to estimate the illuminant from the extracted image patches. To eliminate the effect of limited content in small patches, it uses two additional training features, namely, the mean and the median of the local patches, for illuminant estimation.

Various algorithms that endeavor to mimic the mechanism of the Human Visual System (HVS) using a computational model for color constancy have been presented in the literature [48]–[51]. Gao *et al.* [48] reported a method that is based on the response of Double Opponent (DO) cells to the incident distribution of the color. They apply a *max*- or *sum*-pooling mechanism in long-, medium- and short-wavelength color space to estimate the illuminant color. A biologically inspired computational model was proposed in [50], which depend mainly on center-surround calculations of local contrast to preserve the object color. Their model mimics the coordination between the variable size of the Receptive Field (RF) and its surrounding local contrast by weighting contributions of two overlapping asymmetric Gaussian kernels. Then, the authors estimated the illuminant by modeling higher visual cortical areas according to the local contrasts. A color constancy method that automatically detects the human eyes and extracts the color of the sclera, was proposed by Males *et al.* in [51]. The proposed algorithm assumes that the sclera color contains sufficient accurate information to be used to estimate the scene light color and, hence, reliably color-balance the face image. They reported superior performance compared to other techniques. Nevertheless, the use of this technique is restricted to images that contain at least one reliable human eye.

Although the aforementioned color constancy methods generate reasonably accurate results, to authors' knowledge, the application of image texture for color constancy adjustment of images of scenes illuminated by multiple light sources has not been reported in the literature. With advances in multimedia technologies, there is increased demand for more reliable, accurate and less computation hungry multiple illuminant color constancy techniques. This paper presents Color Constancy Adjustment using the Texture of the Image (CCATI) for single and multiple illuminants. The proposed technique uses a histogram-based algorithm to determine sufficient number of segments for the input image. The proposed algorithm applies an automatic segmentation method that uses the K-means^{++} method to divide the input image into its segments. The proposed technique assumes that each resulting segment represents a dominant light source. The proposed technique then performs entropy analysis on each resulting segment's pixels to extract the texture information of the segment. The resulting texture information is used to choose pixels with sufficient color variations within the segment. Next, the Gray World theorem is applied to compute initial color constancy adjustment factors for each segment using its selected pixels. To balance the effect of different light sources represented by each segment's initial color constancy adjustment factors on each pixel of the image, the proposed method uses Euclidian distance from the pixel to the center of every segment as a measure to regulate and fuse the segments' initial color constancy adjustment factors to calculate the color constancy adjustment factor for that pixel. This ensures that segments which are closer to a given pixel have an increased impact on its final color constancy adjustment factors. Experimental results on two single-illuminant image datasets and two multiple-illuminant image datasets demonstrate that the proposed technique's resulting images exhibit significantly higher color constancy compared to those of the state-of-the-art techniques. The remainder of the paper is structured as follows: Section 2 describes the proposed algorithm, Section 3 discusses the experimental results and the paper will be concluded in Section 4.

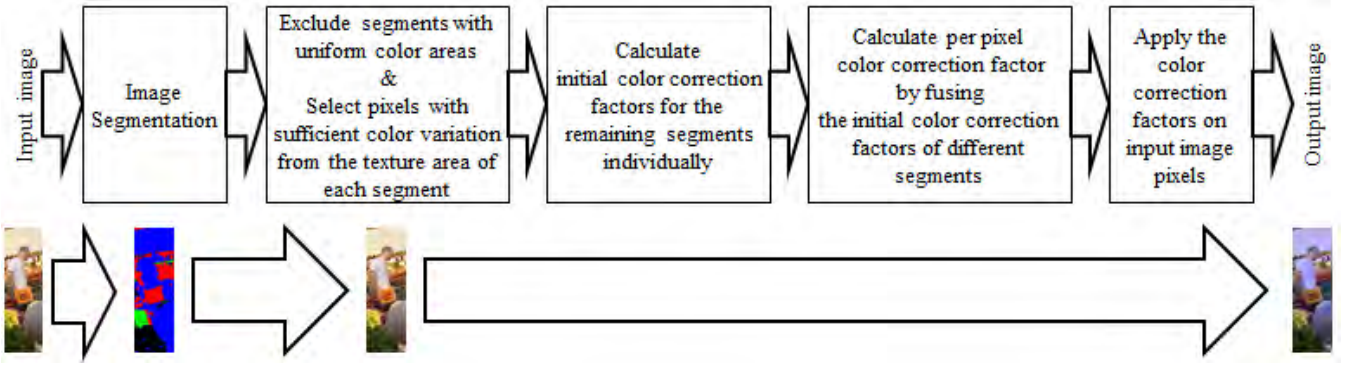

FIGURE 1. An illustrative block diagram of the proposed technique.

II. PROPSOED COLOR CONSTANCY ADJUSTMENT USING IMAGE TEXTURE

Fig. 1 shows an illustrative block diagram of the proposed technique. In this paper, the K-means^{++} algorithm along with a histogram-based method are used to divide the input image into a number of segments. Our investigation shows that entropy analysis of each image segment provides adequate information about the color variations of the pixels. This information is then used to select pixels with sufficient color variation within each segment. The proposed method determines initial color constancy adjustment factors for each segment using its selected pixels. The proposed method assumes each image segment represents a dominant light source. The proposed method then calculates per pixel, color constancy adjustment factors by combining the resulting initial color constancy adjustment factors of different segments adjusted by the Euclidian distances of the pixel from the centroids of the segments. This enables the algorithm to balance the effect of different light sources represented by different segments on each pixel, globally improving overall color constancy of the image. The proposed color constancy adjustment method includes three parts: automatic image segmentation using the K-means^{++} algorithm, calculation of the initial color constancy weighting factors for each segment and computation of the color constancy adjustment weighting factor for each pixel by fusing the color constancy weighting factors of all segments. These three parts are detailed in the following subsections.

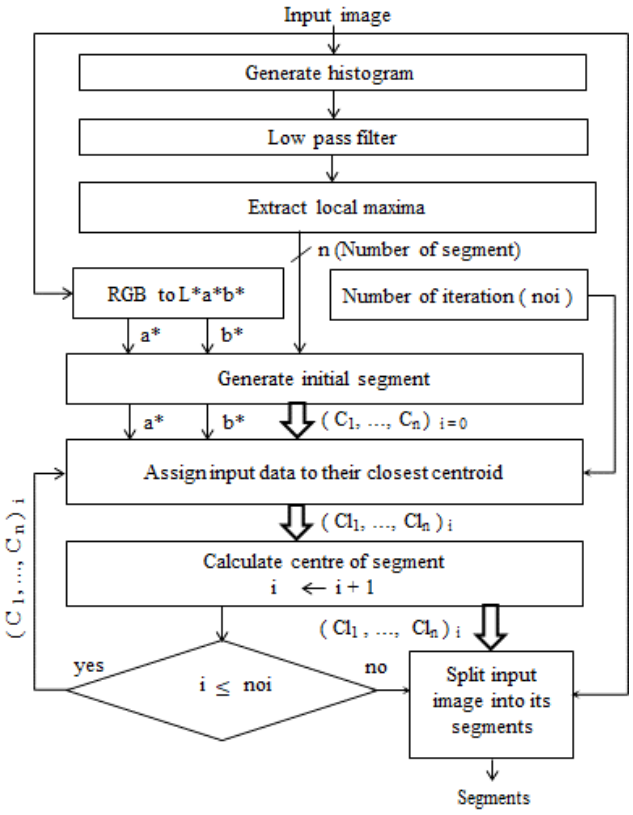

FIGURE 2. Block diagram of the proposed image segmentation algorithm.

A. IMAGE SEGMENTATION USING THE K-MEANS^{++} ALGORITHM

A block diagram of the proposed automatic image segmentation method, which uses the K-means^{++} clustering algorithm [52], is shown in Fig. 2. According to Fig. 2, the algorithm takes an RGB color image and transforms it into a gray scale image. The algorithm uses a histogram-based method to calculate the number of segments demonstrating color diversity areas within image. Hence, it splits the resulting gray scale image data into 256 bins of a histogram. Then, the resulting histogram is smoothed six times using the following Gaussian low-pass filter:

$$[0.25 \quad 0.5 \quad 0.25]$$

The required number of image segments are calculated by counting the number of the local maxima within the smoothed histogram. The presented results are generated by assuming that the distance between two local maxima is greater than 30 and the local maxima height is greater than one thousandth of the total number of image pixels, which was empirically found to generate a reasonable number of segments for representing color variation within the benchmark color constancy

image datasets. The calculated number of segments, which is denoted as n, is shown as n in Fig. 2. Various image segmentation algorithms can be used to split the input image into n segments. However, in this research, the K-means^{++} clustering algorithm, which is simple and effective in dividing the color image into a predefined number of segments according to the variation of the color data, is used. Hence, the input RGB image is converted to the $L^*a^*b^*$ format, where the lightness and the color components of the image are denoted by L*, a* and b*, respectively. The a* and b* color components and the calculated number of the segments n are fed to the K-means^{++} clustering technique.

The K-means^{++} method splits the input image pixels into n segments according to their color variations. The K-means^{++} segmentation method's steps are as follows:

i. Randomly select the initial n centroids of the segments from the a* and b* the input image color component, which are named as $(c_1 \ldots c_n)_{i=0}$, and set i to zero (i denotes the current iteration).
ii. Segment the a* and b* image color components' coefficients into n segments based on their minimum Euclidian distances to the current n centroids, to generate n new segments, which are denoted as $(cl_1 \ldots cl_n)_i$.
iii. Compute the mean value of each resulting segment's coefficients to determine the n new centroids, denoted as $(c_1 \ldots c_n)_i$ in Fig. 2 and increase i by one.
iv. Check if i is larger than the predefined number of iterations, named as noi in Fig. 2. If i is larger than noi, the formerly calculated segments, denoted as $(cl_1 \ldots cl_n)_i$, are the final segments and the segmentation procedure is complete. Change their name to $cl_1 \ldots cl_n$, as shown in Fig. 2, otherwise, back to step ii.

B. TEXTURE EXTRACTION AND CALCULATION OF THE INITIAL CONSTANCY WEIGHTING FACTORS

A block diagram of the proposed texture extraction, segment selection and segment initial color constancy weighting factors computation methods is illustrated in Fig. 3. Each resulting segment from Section 2.1 is processed independently as follows:

i. Calculate the entropy value for each pixel's color components of the segment using 9×9 neighboring values [53] (the entropy value is a statistical measure of the randomness and is used to characterize the texture of the segment).
ii. Normalize and map the resulting entropy values to [0, 1].
iii. Convert each resulting normalized color component segment texture map to binary using two empirical threshold values as detailed in the experimental section.
iv. If all of the resulting binary color component maps are non-zero, calculate its gravitational center and set the segment's relevant bit in the decision vector (DV), a vector indicating which segments have been selected that was initialized to zero.

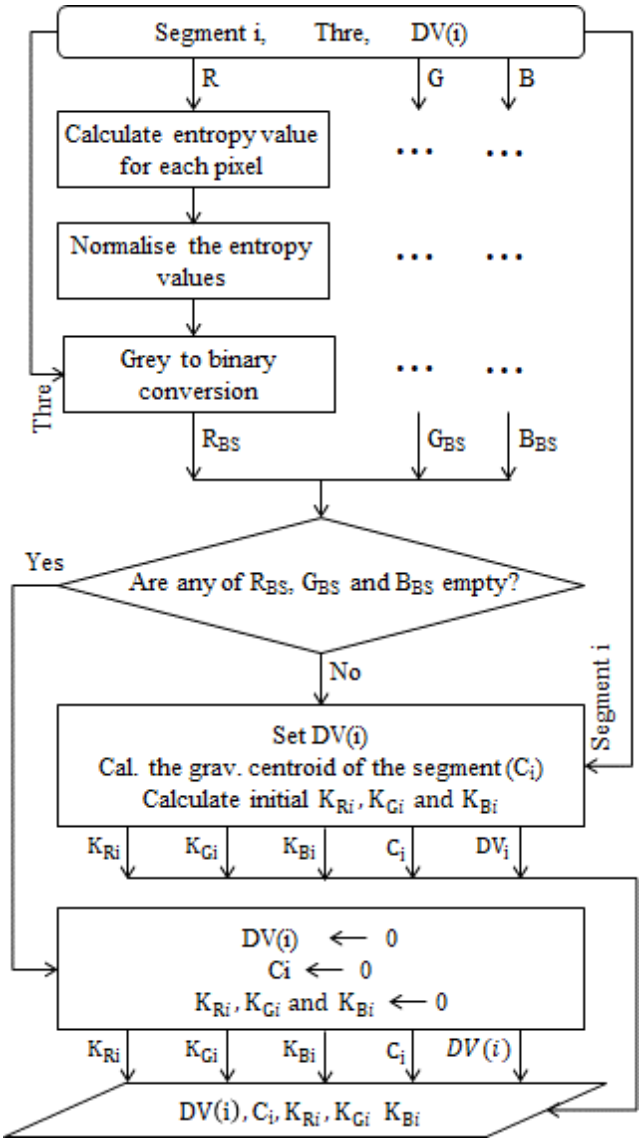

FIGURE 3. Block diagram of the proposed texture extraction, segment selection and segment initial color constancy weighting factor calculation methods.

v. Determine the segment's initial color constancy weighting factors using the input RGB image pixel values, which are identified by the resulting non-zero binary segment's pixels. The weighting factors for the red, green and blue color components are denoted as K_{Ri}, K_{Gi} and K_{Bi}, respectively, in the block diagram, where i represents the segment number. Finally, the Gray World theorem is used to compute the weighting factors, as shown in equation (3):

$$K_{Ci} = SSP_{mean} \Big/ \frac{\sum SSP_C}{N} \tag{3}$$

where K_{Ci} is the initial weighting factor for component $C \in \{R, G, B\}$; SSP_{mean} is the average value of the segment's selected pixel values, which are identified by the non-zero binary segment's pixel values; $\sum SSP_C$ is the sum

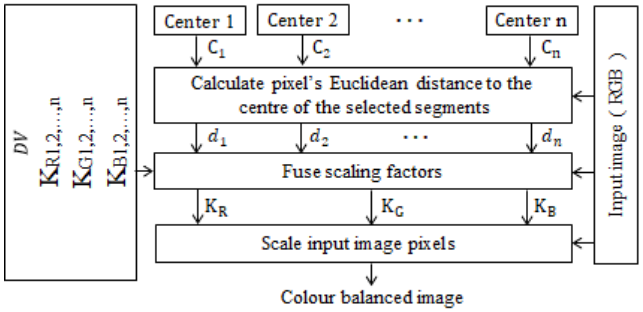

FIGURE 4. Block diagram of the proposed color constancy weighting factor (CCWF) calculation for each pixel by fusing the initial CCWFs of the selected segments.

of component C's segment's selected pixel values; and N is the total number of non-zero binary pixels of the binary segment.

In this research, the Gray World color correction algorithm, which is one of the more effective and yet less computationally expensive techniques compared to other color constancy algorithms [4], [10], [11], [19], [20], is used for simplicity to compute the initial color constancy weighting factors for segments. However, other statistical color constancy methods can be used.

C. CALCULATING THE PER-PIXEL COLOR CONSTANCY WEIGHTING FACTORS

Fig. 4 presents a block diagram of the proposed color constancy adjustment weighting factor calculation method for each pixel. According to Fig. 4, the proposed algorithm takes the segments' centers, which are denoted as $C_{1'}$ $C_{2'}$ $\cdots$, C_n, the RGB input image, the Decision Vector (DV), and the calculated initial color correction weighting factors of all the segments and computes per pixel color correction weighting factors by combining the initial color correction weighting factors of all segments, as explained in the following steps:

i. Calculate the Euclidian distances of the pixel from the centers of all segments, which are denoted as $d_1, d_2, \ldots d_n$ in the block diagram, using equation (4):

$$d_i = \sqrt{\left(x_{C_i} - x_p\right)^2 + \left(y_{C_i} - y_p\right)^2} \tag{4}$$

where x_{C_i} and y_{C_i} are the x and y positions, respectively, of the center of segment i; x_p and y_p represent the x and y positions, respectively, of the pixel in the image; and d_i is the Euclidian distance of the pixel from the center of segment i.

ii. The color constancy adjustment weighting factors for the red, green and blue color component of the pixel, which are denoted as K_R, K_G and K_B, respectively, are calculated by fusing the regulated initial color constancies of the segments using equation (5):

$$K_l = \frac{d_1}{d_1 + d_2 + \cdots + d_n} \times K_{l_1} + \frac{d_2}{d_1 + d_2 + \cdots + d_n} \times K_{l_2} + \cdots + \frac{d_n}{d_1 + d_2 + \cdots + d_n} \times K_{l_n} \tag{5}$$

where K_l is the weighing factor for component l of the pixel; $l \in \{R, G, B\}$; $d_1, d_2, \cdots, d_n$ represent the Euclidian distances of the pixel from the centers of segments 1 to n, respectively, which are denoted as $C_{1'}$ $C_{2'}$ $\cdots$, C_n in the block diagram; and $K_{l'_1}$ $K_{l'_2}$ $\cdots$, K_{l_n} are the initial color constancy weighting factors of color component l of segments 1 to n, respectively.

iii. Scale the R, G and B color components of the input pixel by the resulting color constancy weighting factors using the Von-Kries diagonal model [54], as shown in equation (6):

$$\begin{pmatrix} p\_out_R \\ p\_out_G \\ p\_out_B \end{pmatrix} = \begin{pmatrix} K_R & 0 & 0 \\ 0 & K_G & 0 \\ 0 & 0 & K_B \end{pmatrix} \begin{pmatrix} p_R \\ p_G \\ p_B \end{pmatrix} \tag{6}$$

where p_out_R, p_out_G and p_out_B are the color components of the color-balanced pixel; K_R, K_G and K_B are the calculated weighting factors for the input pixel; and p_R, p_G and p_B are the input pixel's color component values.

III. EXPERIMENTAL RESULTS AND EVALUATION METHODS

The performance of the proposed color correction method for images of scenes, which are lit by a various illuminant is assessed and compared with those of the state-of-the-art techniques using images from four benchmark image datasets. The remainder of this section is organized as follows: the datasets are introduced in sub-section 3.1; sub-section 3.2 explains the assessment criteria; the influence of various factors on the performance of the proposed algorithm is discussed in sub-section 3.3; and sub-section 3.4 details the experimental results.

A. IMAGE DATASETS

B. MULTIPLE-ILLUMINANT DATASETS

1. The Multiple Light Sources dataset (MLS) [32] consists of 9 outdoor images of different sizes, which were captured under two distinct lighting conditions, and 58 indoor images, which were shot under various lighting conditions. The ground truth of the images are also generated using different methods, e.g. by placing several gray balls in the scene and manually correcting the image.
2. The MIMO dataset [33] consists of 58 laboratory and 20 real-world images. The laboratory images were shot under controlled illumination conditions.

C. SINGLE-ILLUMINANT DATASETS

3. The Gray Ball dataset [55], contains 11,340 images from different scenes, where a gray ball is placed in front of the camera. The image of the gray ball is used to assess the scenes' illuminant. Since, there are many neighboring images of the same scene, two hundred images of various scenes and lighting conditions were selected from this dataset for subjective evaluation of the proposed algorithm.

4. The Gehler and Shi image dataset [56] consist of 568 images covering a wide range of indoor and outdoor scenes' images, which were captured under various lighting conditions. A Macbeth color checker chart was located in a known place of each scene, which its image is used to assess the lighting condition of the scene. One hundred images from this dataset are used for subjective evaluation of the proposed color correction method.

D. ASSESSMENT CRITERIA

To evaluate the color constancy of images, both objective and subjective measures are widely used in the literature [1], [33], [40], [57], [58]. Angular error, which is an objective measure, is often used to assess the color constancy of an image when the ground truth of the image is available. In this case, the angular distance between the color-corrected image and its respective ground truth, which is also known as the recovery angular error [59], is determined using equation (7):

$$d_{\theta(recovery)} = \cos^{-1}\left(\frac{e.\hat{e}}{\|e\|\,\|\hat{e}\|}\right) \tag{7}$$

where d_θ represents the angular error, $e.\hat{e}$ indicates the dot product of the ground-truth and the color-corrected image vectors, respectively, and $\|.\|$ denotes the Euclidian norm of the specified vector.

Angular error is the most frequently used measure in assessing the performance of color correction techniques, where the average of the mean or median angular errors of various techniques on a large set of color-balanced images is calculated and used for comparison. The images of an algorithm that has the lowest average of the mean or median angular errors have the highest color constancy.

Recently, Finlayson *et al.* [60] have criticized the application of the (recovery) angular error measure based on the argument that it produces different results for identical scenes viewed under different color light sources. They proposed an improved version of the recovery angular error measure, called reproduction angular error, which is defined as the angle between the image RGB of a white surface when the actual and estimated illuminations are 'divided out'. The reproduction angular error metric can be calculated using equation (8):

$$d_{\theta(reproduction)} = \cos^{-1}\left(\frac{(e/\hat{e})}{\|e/\hat{e}\|}.w\right) \tag{8}$$

where $w = \frac{e/\hat{e}}{\sqrt{3}}$ is the true color of the white reference.

Both recovery and reproduction angular error have been used to assess the objective quality of the color corrected image by computing the average of the mean or median reproduction angular errors of different methods on a large set of color-corrected images and using them for comparison. The images of the method that have the lowest average of the mean or median reproduction angular errors have the highest color constancy.

Although angular error often provides very similar results to human perception, contradictory results have also been reported by researchers in [61], [62]. Since human eyes are the ultimate critic of the color constancy of images, subjective evaluation is considered the most reliable assessment method, regardless of its difficulty in terms of time consumption and required resources. Mean opinion score (MOS) is a subjective measure that is widely used to compare the visual quality of color-balanced images [63], [64]. In this method, a set of images that contain various color variations, objects, and backgrounds and are captured under various light sources are selected and color-balanced by various color constancy adjustment techniques. The resulting images are shown to observers who score the images based on their color constancy. For comparison, the MOS for each algorithm is generated by considering the average scores for the images of a dataset.

According to Fig. 5, the proposed algorithm divided the input image into three segments, where the pixels within each segment are of similar color and the three segments mainly cover leaves, a tree log, and the ball and the blue sky, respectively.

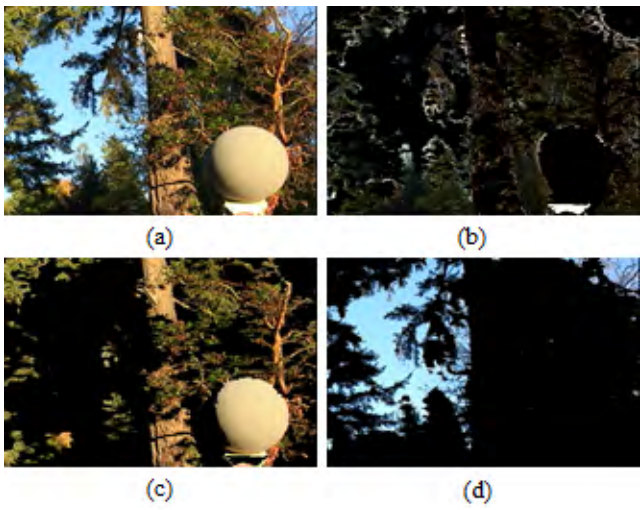

FIGURE 5. Sample outdoor image from the gray ball dataset and its resulting segments that were obtained using the proposed segmentation algorithm: (a) original image and (b-d) the resulting three segments.

According to Fig. 6, which is an indoor image of a scene that is lit by multiple illuminant, the proposed algorithm has split the image into five segments of similar-color areas, which represent the colors of the objects, the colors of the local light sources and the light reflections of various objects that are illuminated by local sources. The experiments were conducted on many sample images from the four datasets that are introduced above. It was visually ascertained that the proposed algorithm determines an acceptable number of segments such that the resulting segments exhibit similar color patches, which is key to the success of the proposed

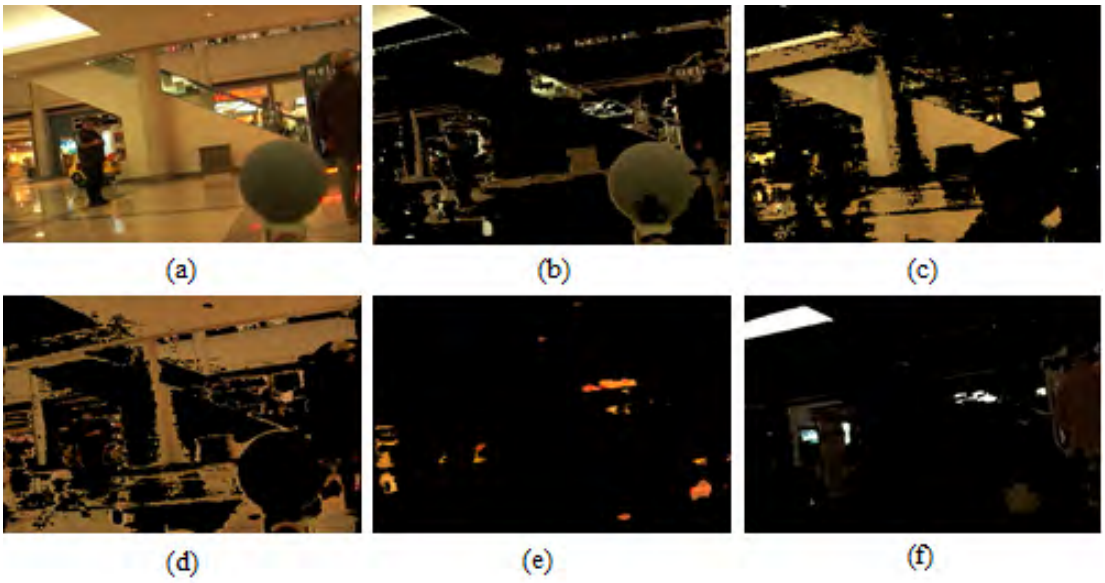

FIGURE 6. Sample indoor image from the gray ball dataset and its resulting segments that were obtained using the proposed segmentation algorithm: (a) original image and (b-f) the resulting five segments.

color correction method. The impact of number of segments on the performance of the proposed color constancy technique will be further investigated in the experimental results section.

E. THRESHOLD SELECTION AND DEMONSTRATION

In the proposed algorithm, as explained in Section 2.2, two threshold values are used to extract pixels with sufficient color variation to be used to calculate the initial color constancy weighting factors for the segment (these thresholds are applied on the normalized gray entropy pixel values of each segment). This operation also excludes pixels of the uniform-color areas from being used for image color constancy adjustment. In general, the existence of a large uniform-color area causes the color-corrected image to be biased to the color of the large uniform area. The range of the threshold values lies between 0 and 1. To empirically determine lower and upper threshold values, which clearly define areas with sufficient color variation, an extensive empirical investigation on a wide range of images of different datasets was conducted. Initial results showed pixels with normalized entropy value less than 0.05 and above 0.95 mainly represent uniform color areas and areas with significant edges, which do not contain adequate color variation. Hence the initial lower and upper threshold values were initialized to 0.05 and 0.95 prior to empirically determine their values precisely.

The following steps were applied to many sample images from the four abovementioned image datasets to empirically determine the two required threshold values, which are named as the upper and lower threshold values and denoted as T_u and T_l, respectively:

i. Assign 0.05 and 0.95 to T_l and T_u, respectively.
ii. Apply the thresholds to the texture of a segment that contains uniform color areas, e.g., blue sky, and set the unselected pixels of the segment to zero.
iii. Visually inspect the resulting segment.
iv. If the uniform-color area of the segment has almost disappeared, go to step vi.
v. Set $T_l = T_l + 0.05$ and $T_u = T_u - 0.05$ and go to step ii.
vi. The current threshold values are the empirical threshold values for this image.

Then, the average of the resulting threshold values for the selected images from the four datasets were calculated and used as the general empirical values for the proposed method, which are 0.3 and 0.7 for T_l and T_u, respectively.

To give a visual sense of the performance of the algorithm, one outdoor image that contains uniform blue sky and one indoor image that contains a uniform-color area were segmented using the proposed algorithm. The entropy values of the segments that contain uniform areas were calculated and the general empirical threshold values were applied. The original images, their uniform-color segments and the resulting selected pixels of the segments are shown in Fig. 7 and Fig. 8. According to Fig. 7c and Fig. 8c, the pixels with adequate color variation are selected by the proposed technique and the uniform-color areas are excluded from contributing to the color constancy correction of the images.

F. EXPERIMENTAL RESULTS

The performance of the proposed Color Constancy Adjustment using the Texture of Image (CCATI) method is assessed and compared with those of the state-of-the-art techniques using the images of the four aforementioned benchmark datasets. This assessment covers both subjective and

FIGURE 7. Sample outdoor image from the gray ball dataset: (a) original image, (b) a segment that contains a uniform-color area, and (c) selected pixels for color constancy adjustment within the segment that represents the non-uniform-color area.

FIGURE 8. Sample indoor image from the gray ball dataset: (a) original image, (b) a segment that contains the uniform-color area, and (c) selected pixels for color constancy adjustment within the segment that represents the non-uniform-color area.

objective evaluation on a wide range of images of scenes that are lit by either a single or multiple light source.

G. SUBJECTIVE RESULTS

To assess and compare the subjective performance of the proposed CCATI algorithm, five sample images from the four image datasets that contain images that were captured under single and multiple light sources in outdoor, indoor, natural and laboratory settings are color-corrected using the proposed CCATI and the state-of-the-art color correction methods. The results are shown in Fig. 9-14. Fig. 9 illustrates a sample image from the Gray Ball dataset, the ground truth of the image, and color-corrected images that were generated using Gray Edge-2, Weighted Gray Edge, Double Opponency and the proposed CCATI method. According to Fig. 9, the proposed method's image exhibits the highest color constancy, whereas the Weighted Gray Edge, Gray Edge-2 and Double Opponency images, in order, have visually lower color corrections, which is inconsistent with their angular errors, which are indicated on the images. To obtain better insight into the achieved color constancy, the gray ball areas of the images that are obtained using the various techniques, which correspond to the area that is highlighted by the red window on the original input image, are shown in Fig. 10. According to Fig. 10a, which shows the gray ball part of the input image, the ball color exhibits a strong yellow color cast compared to its ground truth, as shown in Fig. 10b, which illustrates the true gray color of the ball. The Gray Edge-2 method's image, which is shown in Fig. 10c, exhibits a light brown color cast compared to the ground truth. The Weighted Gray Edge method's image is illustrated in Fig. 10d. This image

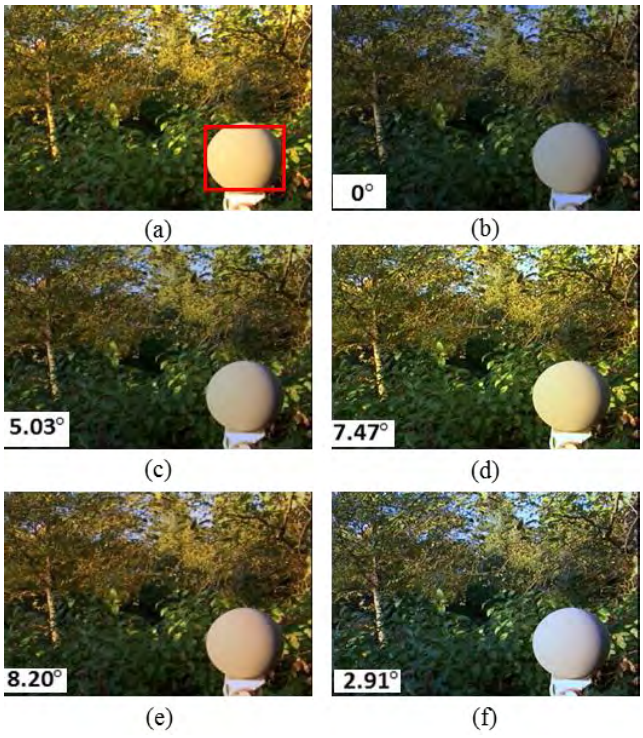

FIGURE 9. Sample image from the gray ball dataset, its ground truth and its color-balanced images: (a) original, (b) ground-truth, (c) Gray Edge-2, (d) Weighted Gray Edge, (e) Double Opponency and (f) the proposed CCATI method's images.

has weaker color cast in comparison to the input image, but still suffers from a high level of yellow color cast. Fig. 10e shows the Double Opponency technique's image. This image

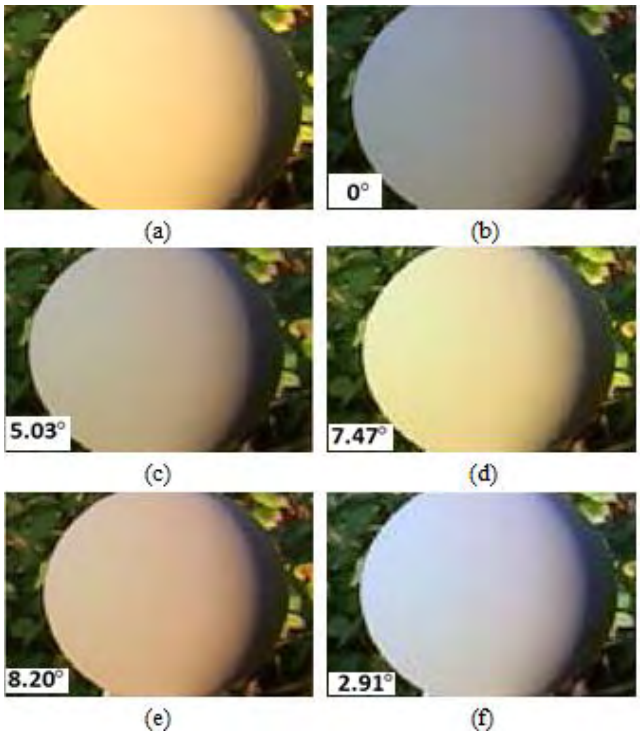

FIGURE 10. Highlighted area of the sample image from the gray ball dataset, its ground truth and its color-balanced images: (a) original image, (b) ground truth, (c) Gray Edge-2, (d) Weighted Gray Edge, (e) Double Opponency and (f) the proposed CCATI method's images.

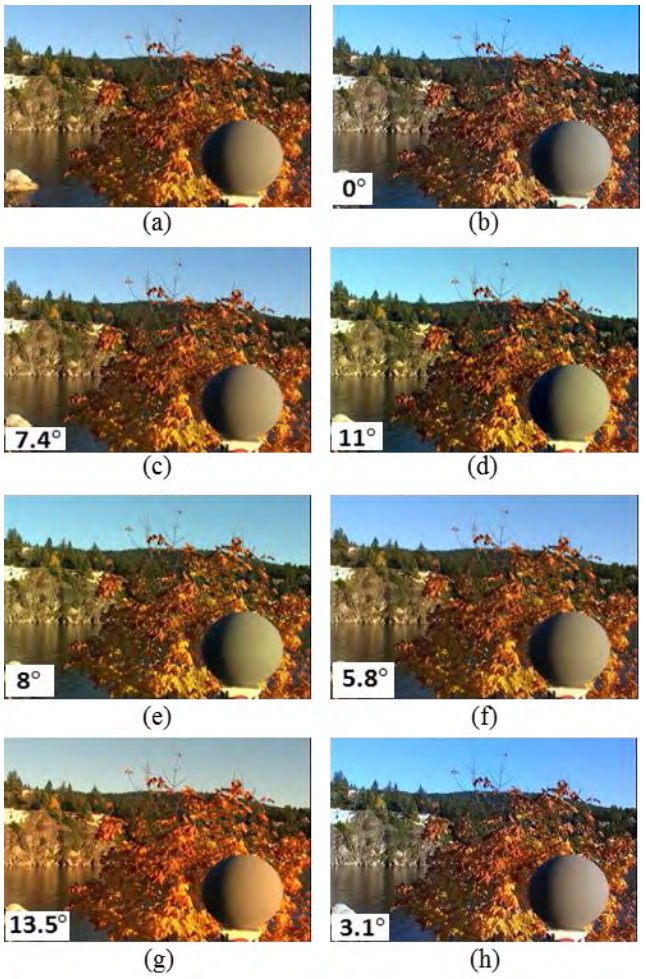

FIGURE 11. Sample image from the gray ball dataset, its ground truth and its color-balanced images: (a) original image, (b) ground truth, (c) Max-RGB, (d) Shades of Gray, (e) Gray Edge-1, (f) Gray Edge-2, (g) Weighted Gray Edge, and (h) Proposed CCATI method's images.

exhibits a high level of orange color cast. Finally, Fig. 10f, which shows the proposed method's image, seems to have the weakest color cast compare to the other methods' images and is the closest to the ground-truth image. Therefore, it is concluded that the proposed CCATI technique's images exhibit the uppermost color corrections compared to the other above-mentioned algorithms.

Fig. 11a and 11b show a sample image from the Gray Ball dataset, which seems to have a yellow color cast, and its ground truth, respectively. A large part of this image is the blue sky, which could degrade the performance of the statistical-based color constancy algorithms. According to Fig. 11c, which shows the Max-RGB method's image, the color cast of the gray ball image, the color cast of the gray ball is very similar to that of the input image. This implies that the Max-RGB algorithm was unable to fully adjust the color of the image. The Shades of Gray algorithm's image, which is shown in Fig. 11d, exhibits significantly weaker color cast compared to the original image, mostly around the gray ball area of the image, whereas the background of image shows higher yellow color cast than the input image. The Gray Edge-1 technique's image, which is shown in Fig. 11e, exhibits a similar color casts to that of the Max-RGB method's image. Although it shows slightly higher color constancy than that of Max-RGB, the gray ball area of its image does not have the pure gray color of the ground-truth image. Fig. 11f shows the Gray Edge-2 method's image. This image demonstrates superior color constancy, and in particular, the area within the gray ball of this image appears to have a reduced level of yellow tint. Nonetheless, the shore and the tree branches still show some levels of color cast. The Weighted Gray Edge methods' image, which is shown in Fig. 11g, exhibits a strong yellow color cast; the gray ball, the tree branch and the shore areas of the image seem to have an extremely strong yellow color cast. The proposed CCATI technique's image is shown in Fig. 11h. This image exhibits the uppermost color correction compared to all the other techniques' images. The color cast from the tree branches, the shore and the gray ball areas of the image is almost removed and the image is closest in color to the ground-truth image.

Fig. 12 illustrate a sample image from the MIMO (real-image group) dataset, its ground truth, and its color-corrected images that are generated using Gray Edge-2, Weighted Gray Edge, Gray Pixel and the proposed CCATI method. According to Fig. 12a, the original image is yellow-color-casted.

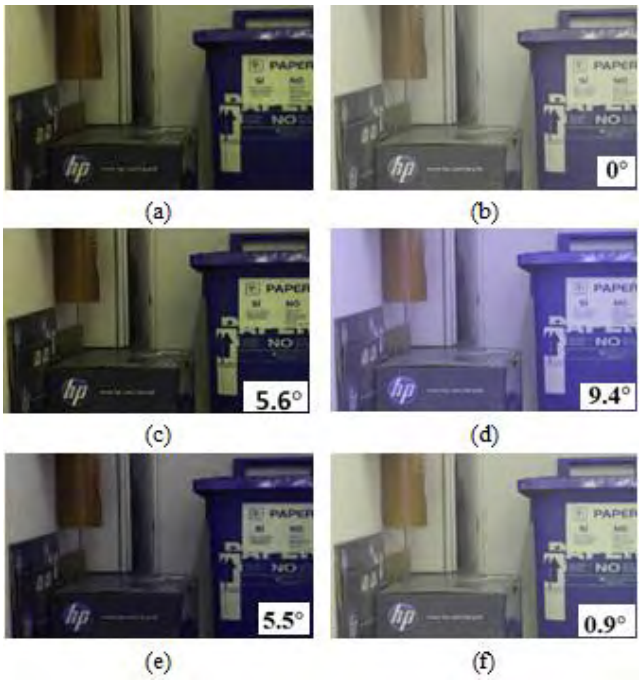

FIGURE 12. Sample image from the MIMO (real-image group) dataset, its ground truth and its color-balanced images: (a) original image, (b) ground truth, (c) Gray Edge-2, (d) Weighted Gray Edge, (e) Gray Pixel and (f) the proposed CCATI method's images.

The Gray Edge-2 algorithm's image, which is shown in Fig. 12c, does not show a noticeable improvement over the original image. The Weighted Gray Edge's image, which is shown in Fig. 12d, exhibits an extremely strong blueish color cast. The Gray Pixel method's image is shown in Fig. 12e. It exhibits significant color correction compared to the Gray Edge-2 and Weighted Grey Edge images, but it still exhibits noticeable differences from the ground-truth image. Fig. 12f shows the proposed CCATI algorithm's image. This image shows uppermost color constancy amongst all the techniques' images, despite its slight yellow color cast. Moreover, the proposed method exhibits the lowest angular error compared to the other techniques' images. Fig. 13 shows two images and their ground truths from the Gehler and Shi dataset and their respected color-corrected images that were generated using Bianco*et al.*'s local-to-global regressor and the proposed CCATI algorithm. The angular error of each image has been calculated and is shown in the lower-left side of each image. According to Fig. 13a, the original images have various levels of green color cast. According to Fig. 13c and Fig. 13d, which illustrate the Bianco *et al.* and the proposed algorithm's images, both methods' images have a low level of blue color cast. However, the proposed method's images show much higher color constancy compared to Bianco *et al.*'s images. By comparing the angular errors of these images, it is concluded that the subjective image quality is in agreement with the objective measures.

Fig. 14 shows an image from the Multiple-Illuminant Light Source dataset, its ground truth and its color-corrected images that were generated using Gray Edge-1, Weighted Gray Edge, Gray Pixel and the proposed CCATI method. According to Fig. 14a, the original image shows a colorful doll that has been placed in front of a multi-colored bag and illuminated by multiple artificial light sources. The luminance of the image background is lower than that of its foreground and parts of the image suffer from red or orange color casts. The Gray Edge-1 technique's image is shown in Fig. 14c. This image exhibits a noticeable reduction of the color cast on its lower-left side; however, the color cast of the image on its lower-right side is evident. Fig. 14d shows the Weighted Gray Edge method's image. This image shows superior color constancy than the Gray Edge-1 method's image; however, it still shows an obvious color cast on its right-hand side. The Gray Pixel technique's image is shown in Fig. 14e. This image appears to have much weaker color cast than

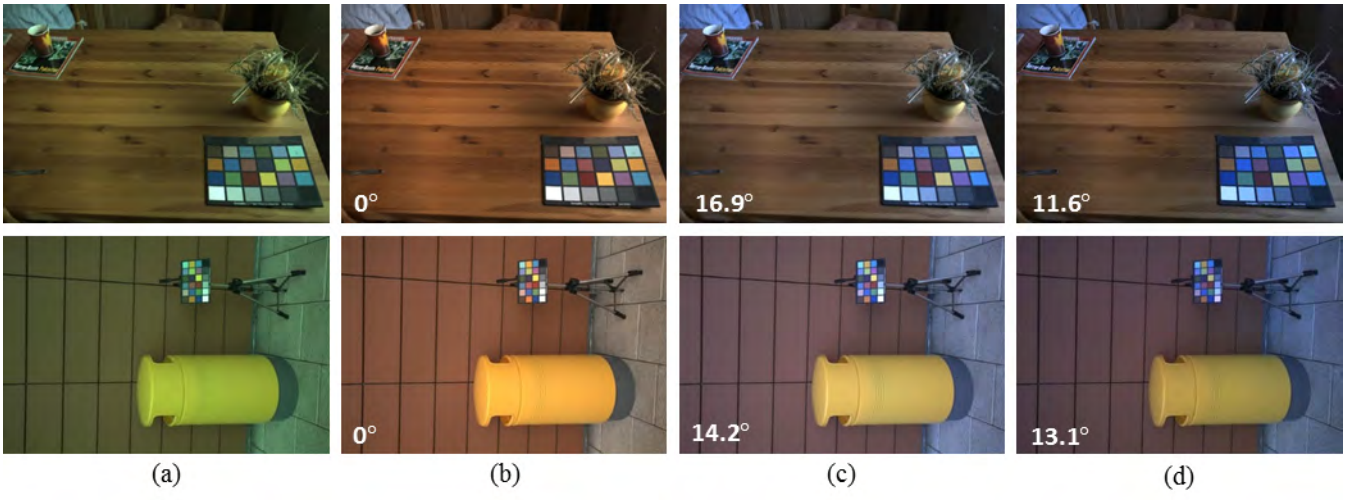

FIGURE 13. Two sample images from the gehler and shi dataset, their ground-truth images and their color-balanced images: (a) original, (b) ground truth, (c) Bianco et al. (local-to-global regressor) and (d) the proposed CCATI method's images.

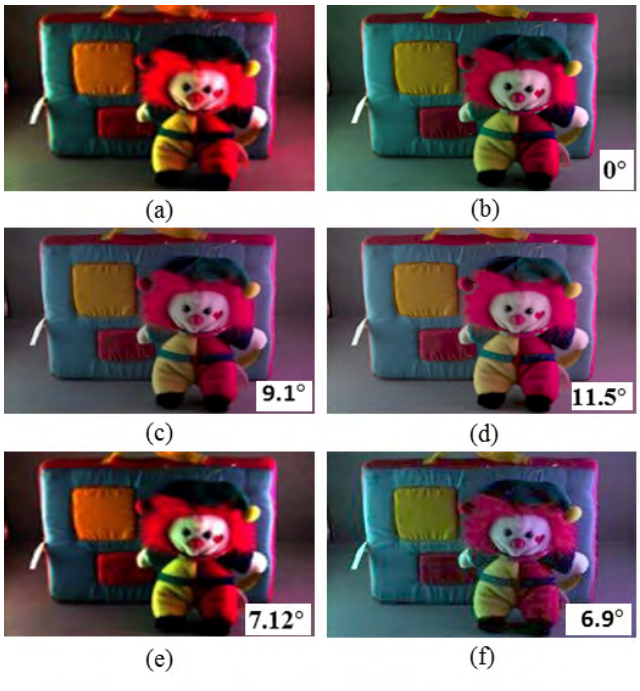

FIGURE 14. Sample image from the multiple-illuminant light source image dataset, its ground truth and its color-balanced images: (a) original image, (b) ground truth, (c) Gray Edge-1, (d) Weighted Gray Edge, (e) Gray Pixel, and (f) the proposed CCATI method's images.

previously explained techniques' images; however, a slight orange color cast on the left side of the image on the carpet and an extreme purple illuminant on the lower-right side of the image are still obvious. The proposed algorithm's image is illustrated in Fig. 14f. The color of the lower-left side of the image seems as if it has been illuminated by a white light. Comparing this image with other techniques' images and the ground truth, it is obvious that the proposed method's image has the closest color constancy to the ground-truth image, despite a slight color cast on the lower-right side of the image. According to the calculated angular errors, which are shown on the images, the proposed image has the lowest angular error, which implies that it has the highest objective quality.

To generate the Mean Opinion Scores (MOSs), 13, 78, 200 and 100 images from the MLS, MIMO, Gray Ball and Gehler and Shi image datasets, respectively, were randomly selected and color-balanced using Weighted Gray Edge (WGE), Gray Pixel, Double Opponency, Convolutional Neural Network

(CNN) and the proposed CCATI techniques. The color-corrected images were shown to 10 viewers, who scored the images on a scale from 1 to 5, where score 5 corresponds to excellent and 1 to unacceptable color constancy of the image. The average of the resulting scores for the images of each dataset and color constancy technique were computed and tabulated in Table 1.

According to Table 1, the proposed method's images have the highest MOSs, which implies that the proposed method's images have the highest subject color constancy amongst the considered techniques' images.

TABLE 1. Mean opinion scores (MOSs) of the propsoed CCATI and weighted gray edge (WGE), gray pixel, double opponency, and convolutional neural network (CNN) algorithms.

		Method			
Dataset (number of images)	WGE	Gray Pixel	Double Opponency	CNN	Proposed
MLS (13 outdoor)	3.25	3.134	4.02	3.26	4.12
MIMO (78)	3.71	4.05	4.11	3.88	4.16
Gray Ball (200)	4.00	3.87	3.813	4.07	4.11
Gehler and Shi (100)	3.80	3.82	3.136	4.05	4.01

H. OBJECTIVE EVALUATION

In this section, the performance of the proposed Color Constancy Adjustment using the Texture of Image (CCATI) method is objectively compared with those of the state-of-the-art techniques using angular error criteria on images from the four aforementioned datasets. In the first part of the experiment, the images of the Gray Ball dataset were color-balanced using the proposed CCATI, the Gray World, the Max-RGB, the Shades of Gray, the 1st- and 2nd-Order Gray Edge, the Pixel-based Gamut Mapping, the Edge-based Gamut Mapping, the Intersection-based Gamut, the Exemplar, the Gray Pixel and the Adaptive Surround Modulation (ASM) color constancy methods. The average mean and median of both recovery and reproduction angular errors of the color-balanced images are tabulated in Table 2. According to Table 2, the proposed CCATI technique's images have the lowest average mean and median recovery and reproduction angular errors amongst all the statistics- and gamut-based color constancy methods, which implies that the proposed technique's images have the uppermost objective color constancies compare to the images of the statistics- and gamut-based techniques. With respect to the learning-based

TABLE 2. Average mean and median angular errors of color constancy methods' images of the gray ball dataset.

	MIMO (real)		MIMO (lab)	
Method	**Mean**	**Median**	**Mean**	**Median**
Statistics-based methods				
Gray world	4.2°	5.2°	3.2°	2.1°
Max_RGB	5.6°	6.8°	7.8°	7.6°
Gray Edge-1	3.1°	5.3°	3.1°	2.8°
Gray Edge-2	4.7°	6.0°	3.2°	2.1°
Proposed CCATI	3.8°	3.8°	2.6°	2.6°
Learning-based methods				
Gijsenij *et al.*	4.2°	3.8°	4.2°	4.8°
MIRF	4.1°	3.3°	2.6°	2.6°
GP(std)(M = 2)	5.7°	3.3°	2.5°	3.1°
GP(std)(M = 4)	5.5°	3.4°	2.3°	2.1°

TABLE 3. Average mean and median angular errors of color constancy methods' images from the mimo dataset.

	Recovery Error		Reproduction Error	
Method	**Mean**	**Median**	**Mean**	**Median**
Statistics-based methods				
Gray World	7.1°	7.0°	10.1°	7.5°
Max_RGB	6.8°	5.3°	9.7°	7.5°
Shades of Gray	6.1°	5.3°	6.9°	3.9°
Gray Edge-1	5.1°	4.7°	6.3°	3.6°
Gray Edge-2	6.1°	4.1°	5.8°	3.6°
Proposed CCATI	4.4°	4.0°	3.9°	3.2°
Gamut-based methods				
Pixel-based Gamut	7.1°	5.8°	4.2°	2.8°
Edge-based Gamut	6.8°	5.8°	4.5°	2.7°
Intersection-based Gamut	6.1°	5.8°	-	-
Learning-based methods				
Exemplar-based	4.4°	3.4°	-	-
Gray Pixel (std)	4.6°	6.2°	-	-
ASM	4.7°	3.8°	5.2°	2.3°

methods, the proposed technique's average mean angular error equals 4.4°, which is equal to the lowest angular error of the learning-based methods. 4.0°. The proposed algorithm's mean reproduction angular error is 3.9°, which is the lowest amongst all techniques and However, the proposed algorithm's average median angular error equals 4.1°, which is slightly higher than that of the best-performing learning-based method, namely, the exemplar-based method, which is the median reproduction angular error is 3.2°, which is lower than those of the statistics and gamut-based methods. This demonstrates that the proposed method's images have very competitive objective results compared to those of the learning-based methods.

In the second part of the experiment, the images of the MIMO dataset were color balanced using the proposed CCATI, the Gray World, Max-RGB and Shades of Gray, 1st- and 2nd Order Gray Edge, Gisenji *et al.*, MIRF and Gray Pixel (GP) color constancy methods. The average mean and median angular errors of the color-corrected real and laboratory images that were obtained via different the various techniques were determined and tabulated in Table 3. From Table 3 it can be seen that the proposed technique's MIMO (real) images have the lowest average median and the second-lowest mean angular errors between the images of the statistics-based techniques. Moreover, the proposed method's MIMO laboratory images exhibit the lowest mean and the second-lowest median angular errors. Hence, it is concluded that the proposed method's images have almost the uppermost objective color constancy compared to those of the statistical-based methods. Compared to those of the learning-based methods, the proposed technique's images have very competitive objective qualities.

Table 4 presents the average median angular errors of the proposed CCATI, the Max-RGB, Gray World, Gray Edge-1, Gray Edge-2 and Gisenji *et al.*methods on 9 outdoor images from the Multiple Light Source dataset. According to this table, the proposed techniques' images have the lowest median angular errors amongst all the techniques. From the objective results that are presented in Tables 2-4, it is concluded that the proposed CCATI method's images exhibit almost the uppermost objective color constancy compared to the images of the other considered techniques.

TABLE 4. Average median angular errors of the proposed CCATI and other color constancy methods on 9 outdoor images from the multiple light source dataset.

Method	Median error
Max-RGB	7.8°
Gray World	8.1°
Gray-Edge-1	6.4°
Gray-Edge-2	5.0°
Gisenji *et al.*	5.1°
Proposed CCATI	4.8°

I. PERFORMANCE EVALUATION FOR A FIXED NUMBER OF SEGMENTS VERSUS AUTOMATIC SEGMENTATION

In this section, it will be empirically shown that the application of the automatic segmentation algorithm significantly improves the performance of the proposed color constancy technique. To do this, the proposed technique, with and without its automatic segmentation method, is applied to the images of the MIMO (real), MIMO (laboratory) and Multiple Light Sources (MLS) (outdoor images) image datasets. The average median angular errors of the resulting images were calculated and are tabulated in Table 5. Results highlight that the proposed method's images have the lowest average angular error when the proposed technique uses its automatic segmentation algorithm rather than a fixed number of segments.

J. COMPUTATIONAL COMPLEXITY

The proposed Color Constancy Adjustment using the Texture of Image (CCATI) and the Grey World color constancy adjustment methods were run on the same Microsoft Windows 10 based personal computer, running on Intel®Core (TM) i3-6006U CPU with 1.99 GHz processor, 4.00 GB of RAM, without any additional dedicated graphic processing unit. These two methods were timed when applied to color balance the images of the MIMO, the Grey Ball and the Color Checker benchmark image datasets. Experimental result show that the proposed technique requires 3.19 times

TABLE 5. Angluar errors of the propsoed method for different numbers of segments.

	Median Angular Error		
Number of Segments (NS)	MIMO (real)	MIMO (lab)	MLS (outdoor)
2	5.13°	6.11°	7.82°
3	5.78°	5.84°	6.14°
4	4.51°	4.14°	5.30°
5	4.14°	3.26°	5.81°
6	6.32°	5.13°	6.57°
Automatic segmentation	3.81°	2.60°	4.82°

more computation time than the benchmark Grey World method.

IV. CONCLUSION

In this paper, the Color Constancy Adjustment using the Texture of Image (CCATI) method was presented. The proposed technique employs a histogram-based method to efficiently calculate the sufficient number of segments for the input image according to the image's color variation. Then, the algorithm applies a K-means^{++} method on the input image, which divides the input image into segments. It determines the entropy of the pixels within each segment and uses it to choose pixels with sufficient color variation for calculating the initial color constancy weighting factors for the segment and reduce the effect of large uniform-color areas on the overall performance of the algorithm. Finally, the proposed CCATI method calculates per pixel color correction adjustment factors by regulating the resulting initial color constancy weighting factors of all segments using the Euclidian distances of the pixel from the centers of gravity of all segments. Experimental results were generated using four benchmark image datasets. The results showed the merit of the proposed technique.

REFERENCES

[1] N. Banić and S. Lončarić, "Color cat: Remembering colors for illumination estimation," *IEEE Signal Process. Lett.*, vol. 22, no. 6, pp. 651–655, Jun. 2013.

[2] G. Schaefer, S. Hordley, and G. Finlayson, "A combined physical and statistical approach to colour constancy," in *Proc. IEEE Comput. Soc. Conf. Comput. Vis. Pattern Recognit.*, vol. 1, Jun. 2005, pp. 148–153.

[3] T. Jiang, D. Nguyen, and K.-D. Kuhnert, "Auto white balance using the coincidence of chromaticity histograms," in *Proc. 8th Int. Conf. Signal Image Technol. Internet Based Syst.*, Naples, Italy, Nov. 2012, pp. 201–208.

[4] A. Gijsenij and T. Gevers, "Color constancy by local averaging," in *Proc. 14th Int. Conf. Image Anal. Process. Workshops (ICIAPW)*, Modena, Italy, Sep. 2007, pp. 171–174.

[5] J. Simão, H. J. A. Schneebeli, and R. F. Vassallo, "An iterative approach for color constancy," in *Proc. Joint Conf. Robot., SBR-LARS Robot. Symp. Robocontrol*, Sao Carlos, Brazil, Oct. 2014, pp. 130–135.

[6] H. R. V. Joze and M. S. Drew, "White patch gamut mapping colour constancy," in *Proc. 19th IEEE Int. Conf. Image Process.*, Orlando, FL, USA, Sep. 2012, pp. 801–804.

[7] S. J. J. Teng, "Robust algorithm for computational color constancy," in *Proc. Int. Conf. Technol. Appl. Artif. Intell.*, Hsinchu, Taiwan, Nov. 2014, pp. 1–8.

[8] M. A. Hussain and A. S. Akbari, "Color constancy adjustment using sub-blocks of the image," *IEEE Access*, vol. 6, pp. 46617–46629, 2018.

[9] G. Buchsbaum, "A spatial processor model for object colour perception," *J. Franklin Inst.*, vol. 310, no. 1, pp. 1–26, Jul. 1980.

[10] S.-C. Tai, T.-W. Liao, Y.-Y. Chang, and C.-P. Yeh, "Automatic white balance algorithm through the average equalization and threshold," in *Proc. 8th Int. Conf. Inf. Sci. Digit. Content Technol.*, Jun. 2012, pp. 571–576.

[11] A. Gijsenij, T. Gevers, and J. Van de Weijer, "Computational color constancy: Survey and experiments," *IEEE Trans. Image Process.*, vol. 20, no. 9, pp. 2475–2489, Sep. 2011.

[12] E. H. Land, "The retinex theory of color vision," *Sci. Amer.*, vol. 237, no. 6, pp. 108–129, Dec. 1977.

[13] E. Y. Lam, "Combining gray world and retinex theory for automatic white balance in digital photography," in *Proc. 9th Int. Symp. Consum. Electron., (ISCE)*, Jun. 2005, pp. 134–139.

[14] N. Banić and S. Lončarić, "Improving the white patch method by subsampling," in *Proc. IEEE Int. Conf. Image Process. (ICIP)*, Paris, France, Oct. 2014, pp. 605–609.

[15] G. D. Finlayson and E. Trezzi, "Shades of gray and colour constancy," in *Proc. IST/SID Color Imag. Conf.*, vol. 1, Jan. 2004, pp. 37–41.

[16] M. A. Hussain, A. Sheikh Akbari, and B. Mallik, "Colour constancy using sub-blocks of the image," in *Proc. Int. Conf. Signals Electron. Syst. (ICSES)*, Krakow, Poland, Sep. 2016, pp. 113–117.

[17] M. A. Hussain, A. Sheikh Akbari, and A. Ghaffari, "Colour constancy using K-means clustering algorithm," in *Proc. 9th Int. Conf. Develop. eSyst. Eng. (DeSE)*, Liverpool, U.K., Aug. 2016, pp. 283–288.

[18] M. A. Hussain and A. S. Akbari, "Max-RGB based colour constancy using the sub-blocks of the image," in *Proc. 9th Int. Conf. Develop. eSyst. Eng. (DeSE)*, Liverpool, U.K., Aug. 2016, pp. 289–294.

[19] J. van de Weijer, T. Gevers, and A. Gijsenij, "Edge–based color constancy," *IEEE Trans Image Process.*, vol. 16, no. 9, pp. 2207–2214, Sep. 2007.

[20] A. Gijsenij, T. Gevers, and J. Van de Weijer, "Improving color constancy by photometric edge weighting," *IEEE Trans. Pattern Anal. Mach. Intell.*, vol. 34, no. 5, pp. 918–929, May 2012.

[21] D. A. Forsyth, "A novel algorithm for color constancy," *Int. J. Comput. Vis.*, vol. 5, no. 1, pp. 5–35, Aug. 1990.

[22] G. D. Finlayson, S. D. Hordley, and I. Tastl, "Gamut constrained illuminant estimation," *Int. J. Comput. Vis.*, vol. 67, no. 1, pp. 93–109, Apr. 2006.

[23] G. Finlayson and S. Hordley, "Improving gamut mapping color constancy," *IEEE Trans. Image Process.*, vol. 9, no. 10, pp. 1774–1783, Oct. 2000.

[24] M. Mosny and B. Funt, "Cubical gamut mapping colour constancy,"in *Proc. Conf. Colour Graph., Imag., Vis.*, Jan. 2014, pp. 466-470.

[25] H.-C. Lee, "Method for computing the scene-illuminant chromaticity from specular highlights," *J. Opt. Soc. Amer. A, Opt. Image Sci.*, vol. 3, no. 14, pp. 1694–1699, Oct. 1986.

[26] S. Tominaga and B. A. Wandell, "Standard surface-reflectance model and illuminant estimation," *J. Opt. Soc. Amer. A, Opt. Image Sci.*, vol. 6, no. 4, pp. 576–584, Apr. 1989.

[27] Y.-Y. Liao, J.-S. Lin, and S.-C. Tai, "Color balance algorithm with zone system in color image correction," in *Proc. 6th Int. Conf. Comput. Sci. Converg. Inf. Technol. (ICCIT)*, Seogwipo-Si, South Korea, Nov. 2011, pp. 167–172.

[28] S.-M. Woo, S.-H. Lee, J.-S. Yoo, and J.-O. Kim, "Improving color constancy in an ambient light environment using the phong reflection model," *IEEE Trans. Image Process.*, vol. 27, no. 4, pp. 1862–1877, Apr. 2018.

[29] M. A. Hussain and A. S. Akbari, "Color constancy algorithm for mixed-illuminant scene images," *IEEE Access*, vol. 6, pp. 8964–8976, 2018.

[30] C. Riess, E. Eibenberger, and E. Angelopoulou, "Illuminant color estimation for real-world mixed-illuminant scenes," in *Proc. IEEE Int. Conf. Comput. Vis. Workshops (ICCV)*, Nov. 2011, pp. 782–789.

[31] M. Bleier, C. Riess, S. Beigpour, E. Eibenberger, E. Angelopoulou, T. Tröger, and A. Kaup, "Color constancy and non-uniform illumination: Can existing algorithms work," in *Proc. IEEE Int. Conf. Comput. Vis. Workshops (ICCV)*, Nov. 2011, pp. 774–781.

[32] A. Gijsenij, R. Lu, and T. Gevers, "Color constancy for multiple light sources," *IEEE Trans. Image Process.*, vol. 21, no. 2, pp. 697–707, Feb. 2012.

[33] S. Beigpour, C. Riess, J. van de Weijer, and E. Angelopoulou, "Multi-illuminant estimation with conditional random fields," *IEEE Trans. Image Process.*, vol. 23, no. 1, pp. 83–96, Jan. 2014.
[34] L. Mutimbu and A. Robles-Kelly, "Multiple illuminant color estimation via statistical inference on factor graphs," *IEEE Trans. Image Process.*, vol. 25, no. 11, pp. 5383–5396, Nov. 2016.
[35] K.-F. Yang, S.-B. Gao, and Y.-J. Li, "Efficient illuminant estimation for color constancy using grey pixels," in *Proc. IEEE Conf. Comput. Vis. Pattern Recognit. (CVPR)*, Jun. 2015, pp. 2254–2263.
[36] B. Mazin, J. Delon, and Y. Gousseau, "Estimation of illuminants from projections on the planckian locus," *IEEE Trans. Image Process.*, vol. 24, no. 6, pp. 1944–1955, Jun. 2015.
[37] S. Bianco and R. Schettini, "Adaptive color constancy using faces," *IEEE Trans. Pattern Anal. Mach. Intell.*, vol. 36, no. 8, pp. 1505–1518, Aug. 2014.
[38] N. Elfiky, T. Gevers, A. Gijsenij, and J. Gonzàlez, "Color constancy using 3D scene geometry derived from a single image," *IEEE Trans. Image Process.*, vol. 23, no. 9, pp. 3855–3868, Sep. 2014.
[39] D. Cheng, B. Price, S. Cohen, and M. S. Brown, "Beyond white: Ground truth colors for color constancy correction," in *Proc. IEEE Int. Conf. Comput. Vis. (ICCV)*, Santiago, Chile, Dec. 2013, pp. 298–306.
[40] D. Cheng, A. Kamel, B. Price, S. Cohen, and M. S. Brown, "Two illuminant estimation and user correction preference," in *Proc. IEEE Conf. Comput. Vis. Pattern Recognit. (CVPR)*, Jun. 2016, pp. 469–477.
[41] S.-H. Lee, S.-M. Woo, J.-H. Choi, and J.-O. Kim, "Two-step multi-illuminant color constancy for outdoor scenes," in *Proc. IEEE Int. Conf. Image Process. (ICIP)*, Beijing, China, Sep. 2017, pp. 710–714.
[42] S. Bianco, C. Cusano, and R. Schettini, "Color constancy using CNNs," in *Proc. IEEE Conf. Comput. Vis. Pattern Recognit. Workshops (CVPRW)*, Jun. 2015, pp. 81–89.
[43] J. T. Barron, "Convolutional color constancy," in *Proc. IEEE Int. Conf. Comput. Vis. (ICCV)*, Jun. 2015, pp. 379–387.
[44] H. R. V. Joze and M. S. Drew, "Exemplar-based color constancy and multiple illumination," *IEEE Trans. Pattern Anal. Mach. Intell*, vol. 36, no. 5, pp. 860–873, May 2014.
[45] D. Fourure, R. Emonet, E. Fromont, D. Muselet, A. Trémeau, and C. Wolf, "Mixed pooling neural networks for color constancy," in *Proc. IEEE Int. Conf. Image Process.*, Phoenix, AZ, USA, Sep. 2016, pp. 3997–4001.
[46] S. Bianco, C. Cusano, and R. Schettini, "Single and multiple illuminant estimation using convolutional neural networks," *IEEE Trans. Image Process.*, vol. 26, no. 9, pp. 4347–4362, Sep. 2017.
[47] C. Aytekin, J. Nikkanen, and M. Gabbouj, "Deep multi-resolution color constancy," in *Proc. IEEE Int. Conf. Image Process. (ICIP)*, Beijing, China, Sep. 2017, pp. 3735–3739.
[48] S.-B. Gao, K.-F. Yang, C.-Y. Li, and Y.-J. Li, "Color constancy using double-opponency," *IEEE Trans. Pattern Anal. Mach. Intell.*, vol. 37, no. 10, pp. 1973–1985, Oct. 2013.
[49] X.-S. Zhang, S.-B. Gao, R.-X. Li, X.-Y. Du, C.-Y. Li, and Y.-J. Li, "A retinal mechanism inspired color constancy model," *IEEE Trans. Image Process.*, vol. 25, no. 3, pp. 1219–1232, Mar. 2016.
[50] A. Akbarinia and C. A. Parraga, "Color constancy beyond the classical receptive field," *IEEE Trans. Pattern Anal. Mach. Intell.*, vol. 40, no. 9, pp. 2081–2094, Sep. 2018.
[51] M. Males, A. Hedi, and M. Grgic, "Colour balancing using sclera colour," *IET Image Process.*, vol. 12, no. 3, pp. 416–421, Mar. 2018.
[52] D. Arthur and S. Vassilvitskii, "K-means++: The advantages of careful seeding," in *Proc. 18th Annu. ACM-SIAM Symp. Discrete Algorithms*, 2007, pp. 1027–1035.
[53] R. C. Gonzalez, R. E. Woods, and S. L. Eddins, "Representation and description," in *Digital Image Processing Using MATLAB*. Upper Saddle River, NJ, USA: Prentice-Hall, 2003, ch. 11, pp. 464–4613.
[54] J. von Kries, "Influence of adaptation on the effects produced by luminous stimuli," in *Sources of Color Science*, D. L. MacAdam, Ed. Cambridge, MA, USA: MIT Press, 1970, pp. 109–119.
[55] F. Ciurea and B. Funt, "A large image database for color constancy research," in *Proc. 11th Color Imag. Conf. Imag. Sci. Technol.*, Jan. 2003, pp. 160–164.
[56] P. V. Gehler, C. Rother, A. Blake, T. Minka, and T. Sharp, "Bayesian color constancy revisited," in *Proc. IEEE Conf. Comput. Vis. Pattern Recognit. (CVPR)*, Jun. 2008, pp. 1–8.
[57] S. Wang, Y. Zhang, P. Deng, and F. Zhou, "Fast automatic white balancing method by color histogram stretching," in *Proc. 4th Int. Congr. Image Signal Process.*, Shanghai, China, Oct. 2011, pp. 979–983.
[58] B. Zhang and A. U. Batur, "A real-time auto white balance algorithm for mobile phone cameras," in *Proc. IEEE Int. Conf. Consum. Electron. (ICCE)*, Las Vegas, NV, USA, Jan. 2012, pp. 1–4.
[59] S. D. Hordley and G. D. Finlayson, "Re-evaluating color constancy algorithms," in *Proc. 17th Int. Conf. Pattern Recognit.*, vol. 1, Aug. 2004, pp. 76–79.
[60] G. D. Finlayson, R. Zakizadeh, and A. Gijsenij, "The reproduction angular error for evaluating the performance of illuminant estimation algorithms," *IEEE Trans. Pattern Anal. Mach. Intell.*, vol. 39, no. 7, pp. 1482–1488, Jul. 2017.
[61] L. Shi, W. Xiong, and B. Funt, "Illumination estimation via thin-plate spline interpolation," *J. Opt. Soc. Amer. A, Opt. Image Sci.*, vol. 28, no. 5, pp. 940–948, 2011.
[62] A. Gijsenij, T. Gevers, and M. P. Lucassen, "Perceptual analysis of distance measures for color constancy algorithms," *J. Opt. Soc. Amer. A, Opt. Image Sci.*, vol. 26, no. 10, pp. 2243–2256, 2009.
[63] S. Bianco, L. Celona, P. Napoletano, and R. Schettini, "On the use of deep learning for blind image quality assessment," *Signal, Image Video Process.*, vol. 12, no. 2, pp. 355–362, Feb. 2018.
[64] R. C. Streijl, S. Winkler, and D. S. Hands, "Mean opinion score (MOS) revisited: Methods and applications, limitations and alternatives," *Multimedia Syst.*, vol. 22, no. 2, pp. 213–227, Mar. 2016.

MD AKMOL HUSSAIN received the B.Eng. degree in electronics and communication from the University of Wolverhampton, in 2011, and the master's degree (Mainly by Research) from the University of Gloucestershire, in 2014. He is currently pursuing the Ph.D. degree with Leeds Beckett University, U.K. His research interests include computer vision, image processing, and image forensics.

AKBAR SHEIKH-AKBARI received the B.Sc. (Hons.), M.Sc. (Distinction), and Ph.D. degrees in electronic and electrical engineering, 1992, 1995, and 2005, respectively. After completing the Ph.D. degree at the University of Strathclyde in the field of stereo/multi-view video processing, he continued his career in industry, worked on real-time embedded video analytics systems. He is currently a Senior Lecturer with the School of Computing, Creative Technologies & Engineering, Leeds Beckett University. His main research interests include signal processing, hyperspectral image processing, source camera identification, image/video forgery, image hashing, biometric identification techniques, assisted living technologies, compressive sensing, camera tracking using retro-reflective materials, standard and non-standard image/video codecs, e.g., H.264 and HEVC, multi-view image/video processing, color constancy techniques, resolution enhancement methods, edge detection in low-SNR environments, and medical image processing.

EDWARD ABBOTT HALPIN has led and participated in many international and multi-disciplinary, multi-partner research projects, since 1990. He has acted as an expert for the European Parliament Scientific and Technical Options Assessment (STOA) Unit, examining and evaluating innovative research areas. He is currently an Associate Schumann Fellow of European University, Florence, and also with Leeds Beckett University. His work on developing the feasibility, evaluation, and impact for a speculative innovation project, relating to a Missing Children Alert System for Plan International worth $4,000,000, involved multi-stakeholder engagement including work with the Governments of India, Nepal, Bangladesh, the South Asian Area for Regional Cooperation and many local and NGO communities. He is an Expert Panel Member with the Cambridge Governance Labs, Cambridge University, and a Visiting Professor with Open University.